RSC Advances

PAPER

View Article Online
View Journal | View Issue

Cite this: *RSC Adv.*, 2026, **16**, 8226

Enhanced environmental remediation through hybrid adsorption-photocatalysis using ZnO/TiO_2-CaAlg composite catalysts

Nesrine Ammouchi,[a] Abdallah Zaiter,[b] Atmane Djermoune,[c] Nawal Bouzenad,[d] Nada Hamrouche,[d] Amdjed Abdennouri,[d] Youghourta Belhocine,[d] Najoua Sbei,[e] Seyfeddine Rahali,[f] Tarek H. Taha,[g] Fehmi Boufahja,[g] Walid Elfalleh,[g] Stefania Garzoli,*[h] Hamdi Bendif[g] and Djihane Slimane Ben Ali[i]

Due to the toxic, carcinogenic, and environmentally persistent nature of dyes such as crystal violet, water pollution resulting from industrial dye discharges has become a critical global environmental issue. This study investigates a hybrid approach to address water pollution by integrating adsorption and advanced oxidation processes (AOPs) using ZnO/TiO_2-CaAlg as a catalyst. Sodium alginate, a naturally occurring biopolymer, was employed as the support matrix for the catalyst, taking advantage of its hydrophilic nature, biocompatibility, and ability to form strong electrostatic interactions with cationic dyes. Key parameters such as dye concentration, catalyst dosage, hydrogen peroxide volume, and solution pH were optimized to maximize degradation efficiency. Both individual and combined processes were evaluated to assess the synergistic effects on dye removal. The stability and reusability of the catalyst were evaluated, demonstrating its potential as a scalable and environmentally sustainable solution for wastewater treatment. The findings underscore the potential of ZnO/TiO_2-CaAlg catalysts in mitigating persistent organic pollutants, contributing to the development of advanced treatment methods for environmental remediation.

Received 7th December 2025
Accepted 3rd February 2026

DOI: 10.1039/d5ra09465h

rsc.li/rsc-advances

1. Introduction

Water contamination by synthetic dyes represents a major global environmental concern, particularly due to large-scale discharges from textile, cosmetic, pharmaceutical, plastic, and pulp industries.[1–5] Owing to their complex molecular structures, dyes are often highly stable, toxic, and potentially carcinogenic or mutagenic, leading to severe risks for both human health and aquatic ecosystems.[6,7]

Crystal violet (CV), a cationic triphenylmethane dye, is widely used in microbiology for Gram staining, as well as in histological and pharmaceutical applications.[8,9] Despite its usefulness, CV is resistant to degradation and exhibits significant toxicity toward living organisms, causing irritation, tissue damage, and adverse ecological effects when released untreated into water bodies.[10,11] For these reasons, crystal violet is frequently selected as a model pollutant in dye-removal studies.

Conventional wastewater treatment methods, such as coagulation, filtration, and adsorption, are commonly applied to dye-containing effluents.[12–15] However, these approaches often fail to achieve complete removal of recalcitrant organic pollutants and may generate secondary contamination problems.[16] In this context, advanced oxidation processes (AOPs), including photocatalysis, have emerged as effective alternatives due to their ability to generate highly reactive species, particularly hydroxyl radicals (˙OH), capable of degrading persistent organic compounds.[17,18] More recently, hybrid systems combining adsorption and AOPs under a "capture and destroy" strategy have attracted increasing attention for enhancing pollutant removal efficiency while minimizing secondary waste.[19–21]

Among photocatalysts, metal oxides such as TiO_2 and ZnO are widely investigated owing to their strong oxidative potential and chemical stability.[22–24] Nevertheless, the practical application of suspended photocatalyst particles is limited by difficulties related to recovery, reuse, and scalability, as well as by low quantum

[a]*Laboratory for Research on the Physico-Chemistry of Surfaces and Interfaces (LRPCSI), Department of Sciences and Technology, Faculty of Technology, University 20 August 1955, Skikda 21000, Algeria*

[b]*Laboratory of Applied Chemistry and Materials Technology, Larbi Ben M'Hidi-Oum El Bouaghi University, Oum El Bouaghi, 04000, Algeria*

[c]*Scientific and Technical Research Center in Physical and Chemical Analyses, BP 384 Bou-Ismail, RP 42004 Tipaza, Algeria*

[d]*Laboratory of Catalysis, Bioprocesses and Environment (LCBE), University 20 August 1955 Skikda 21000, Algeria*

[e]*Department of Organic Chemistry, University of Alcalá, 28871, Alcalá de Henares, Madrid, Spain*

[f]*Department of Chemistry, College of Science, Qassim University, Buraydah, Saudi Arabia*

[g]*Department of Biology, College of Science, Imam Mohammad Ibn Saud Islamic University (IMSIU), Riyadh 11623, Saudi Arabia*

[h]*Department of Chemistry and Technologies of Drug, Sapienza University, P. le Aldo Moro, 5,00185 Rome, Italy. E-mail: stefania.garzoli@uniroma1.it*

[i]*Department of Petrochemical, Faculty of Technology, University of 20 Août1955, El Hadaiek Road, B. O. 26, 21000 Skikda, Algeria*

efficiency and poor visible-light utilization.[25–27] To overcome these drawbacks, immobilization of photocatalysts on suitable support materials has been proposed as a promising solution.[28]

Sodium alginate, a natural biopolymer derived from brown algae, has gained considerable interest as a support material due to its hydrophilicity, biocompatibility, non-toxicity, and low cost.[29–31] In the presence of divalent cations such as Ca^{2+}, alginate forms stable hydrogels *via* the well-known "egg-box" structure, enabling effective immobilization of metal oxide photocatalysts.[32] Moreover, the negatively charged carboxylate groups of alginate promote strong electrostatic interactions with cationic dyes such as crystal violet, enhancing adsorption capacity and overall removal efficiency.[33] Similar advantages have been reported for other natural supports, including chitosan, cellulose derivatives, lignin, natural gums, and clay-based composites, which contribute to improved catalyst stability and pollutant adsorption.[34–40]

In this context, the present study investigates the degradation of crystal violet using ZnO/TiO_2-CaAlg composite catalysts through a hybrid adsorption–photocatalysis–AOP approach. The effects of key operational parameters, including initial dye concentration, catalyst dosage, H_2O_2 volume, and solution pH, are systematically evaluated. The individual and combined contributions of adsorption and photocatalytic oxidation are examined, along with catalyst stability and reusability, to assess the potential of ZnO/TiO_2-CaAlg composites for efficient and sustainable wastewater treatment applications.

2. Materials and methods

2.1. Chemicals

The photocatalysts used in this study include titanium(IV) oxide (anatase powder, 99.8% trace metals basis), obtained from Sigma-Aldrich (USA), and zinc oxide. Formaldehyde (formol) and sulfuric acid were also sourced from Sigma-Aldrich (USA). Calcium chloride dihydrate and Mueller Hinton Agar, both of laboratory reagent-grade materials, were acquired from Merck (Germany), along with sodium carbonate and hydrogen peroxide (30%). Sodium chloride was obtained from VWR International LLC (USA). The dye used for degradation studies was hexamethyl pararosaniline chloride ($C_{35}H_{30}N_3Cl$; M_W = 407.99 g mol^{-1}, 95%), commercially known as crystal violet (CV), also purchased from Merck (Germany). Sodium hydroxide (NaOH, 98.7%) and hydrochloric acid (HCl, 35–37%) solutions, both obtained from Sigma-Aldrich (USA), were used to adjust the pH.

2.2. Collection, identification, and sample preparation of *Sargassum muticum*

Sargassum muticum (Yendo) Fensholt was collected from rocky substrates along the Skikda coastline (Stora, northeastern Algeria; 36°53′54.9″ N, 6°52′48.1″ E) in January 2022 (Fig. 1). The species was identified based on macroscopic and microscopic observations and taxonomic keys.[41] *S. muticum* is a brown macroalga characterized by a flexible thallus, pyramidal fronds with yellow-green to reddish-brown coloration, and air-filled vesicles (aerocysts) that facilitate flotation, commonly found in intertidal and subtidal rocky zones.[42]

The collected biomass was naturally rinsed by seawater to remove epiphytes and debris, then washed with freshwater to eliminate residual salts. To avoid photolytic and thermal degradation, the samples were air-dried in the shade, coarsely ground, and stored in dark sealed containers prior to use.[43]

2.3. Alginate extraction from *Sargassum muticum*

Alginate extraction carried out following the method outlined by Torres *et al.* (2007)[44] with modifications. The algae were

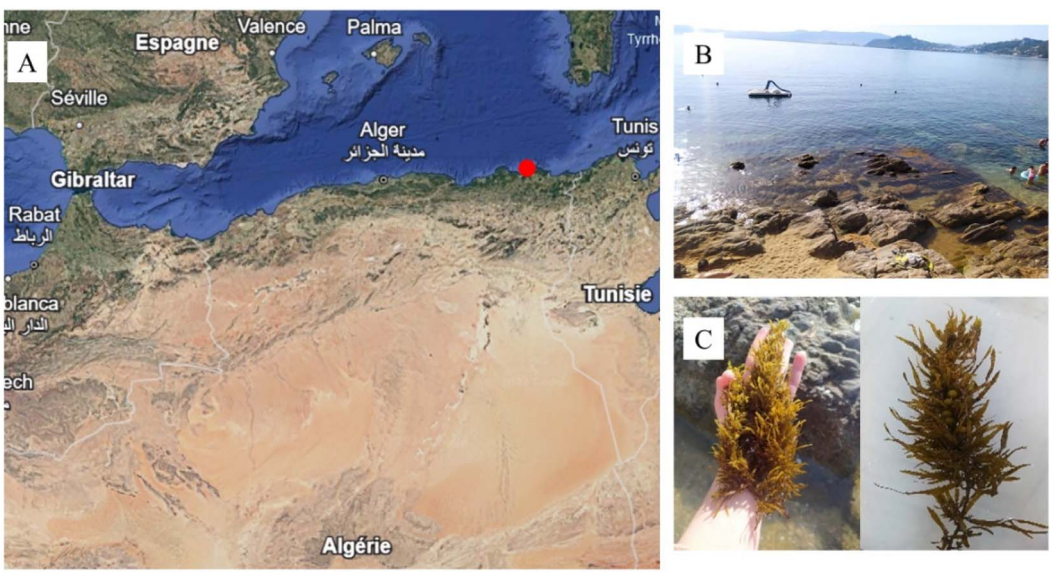

Fig. 1 (a) Geographical location of *Sargassum muticum* on the Skikda coastline (northeastern Algeria); (b) rocky substrates colonized by *Sargassum muticum*; (c) sampling of *Sargassum muticum*.

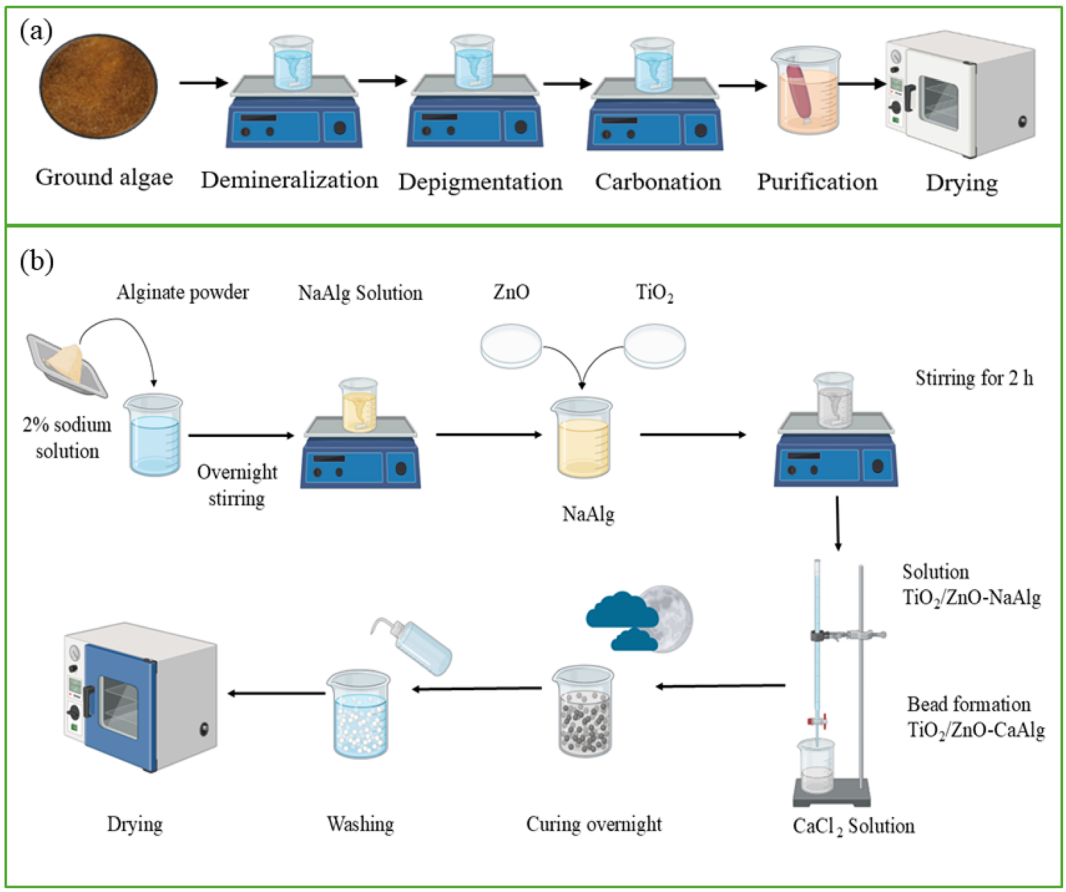

Fig. 2 (a) Schematic illustration of the alginate extraction process; (b) schematic illustration of the TiO_2/ZnO-CaAlg composite preparation process.

immersed in a 2% formaldehyde solution for 24 hours, then washed several times with distilled water and subsequently filtered. The solid residue was placed in 0.02 N sulfuric acid at 60 °C for 2 hours, with continuous stirring (Fig. 2a). After acid treatment, the algae were carefully rinsed with distilled water and filtered. The retrieved substances were then carbonated in a 4% sodium carbonate solution at 60 °C for 2 h, followed by filtration. The filtrate, containing polysaccharides, was dialyzed using a dialysis membrane with a 3500 Da molecular weight cutoff for 48 hours. The resulting material was then dried and preserved.

2.4. Synthesis of TiO_2/ZnO-CaAlg composite beads

TiO_2/ZnO-CaAlg preparation was adapted from the protocol of Albarelli *et al.* (2009) [45] with modifications (Fig. 2b). A 2% sodium alginate (NaAlg) solution agitated continuously overnight. Subsequently, 50 mL of the NaAlg solution were stirred with various proportions of TiO_2/ZnO under constant agitation at 200 rpm. The mass ratios of TiO_2 to ZnO employed were 2 : 2 (equivalent), 2 : 1, and 1 : 2 (non-equivalent). For the 1 : 1 ratio, 1 g of TiO_2 and 1 g of ZnO were used. The mixture containing NaAlg and TiO_2/ZnO was continuously agitated for 2 h. Using a burette, this mixture was gradually introduced into a 50 mL calcium chloride ($CaCl_2$) solution at a concentration of 20 g L^{-1}, under constant agitation. The droplet height was maintained at 5.5 cm to ensure the formation of uniform beads. The TiO_2/ZnO-CaAlg beads were left in the $CaCl_2$ solution overnight to allow for complete formation and hardening. Finally, the beads were washed with distilled water and dried in an oven at 80 °C for 24 to 48 hours.

2.5. Characterization of TiO_2/ZnO-CaAlg composite beads

The chemical composition of the substances was analyzed using FTIR spectroscopy (ATR mode) with a Nicolet IS10 spectrometer (Thermo Fisher Scientific Inc., Waltham, MA, USA), allowing for the identification of functional groups within the materials. XRD analysis, performed with a Thermo Scientific K-Alpha diffractometer (USA) equipped with an Al Kα anode, to determine the crystalline structure and phase composition. Diffraction patterns were recorded over a 2θ range of 10° to 80°. SEM imaging, conducted with a JEOL JSM-IT800 microscope (JEOL Ltd, Tokyo, Japan), provided high-resolution views of the materials' microstructure, while EDX analysis using a Bruker detector (Bruker Corporation, Karlsruhe, Germany) on a Quanta 650 FEG microscope (Thermo Fisher Scientific, USA), revealed the spatial distribution of elements. These complementary techniques provided a comprehensive understanding of the materials' structural and compositional properties.

2.6. Preparation of stock and working solutions of CV

A stock solution of CV, with the chemical formula $C_{25}H_{30}N_3Cl$, was prepared by dissolving 0.1 g of CV powder in distilled water, with continuous agitation until complete dissolution. This resulted in a stock solution with a concentration of 1 g L^{-1}. Using this stock solution, diluted solutions of 10 ppm, 25 ppm, and 50 ppm were prepared according to the dilution formula (eqn (1)).

$$C_1V_1 = C_2V_2 \quad (1)$$

2.7. Preparation of hydrogen peroxide (H_2O_2) solution

To prepare a 1 mol L^{-1} hydrogen peroxide (H_2O_2) solution, a concentrated H_2O_2 solution at 30% (approximately 9.8 mol L^{-1}) was used. A precise 10 mL volume of the concentrated solution was measured using a graduated pipette and transferred into a 100 mL volumetric flask. Distilled water was then added to the flask up to the calibration mark to achieve a final volume of 100 mL.

2.8. Evaluation of sequential adsorption–photocatalysis and advanced oxidation processes

2.8.1. Sequential adsorption and photocatalysis. All experiments were designed according to a two-step protocol to decouple adsorption phenomena from photocatalytic degradation. In a typical experiment, a predetermined mass of ZnO/TiO_2-CaAlg composite beads was introduced into 300 mL of an aqueous CV solution and magnetically stirred at 200 rpm for 30 min under dark conditions to allow adsorption while preventing any photocatalytic reaction.

Following the dark adsorption phase, the suspension was transferred to the photocatalytic chamber and exposed to UV irradiation (254 nm) for 50 min under continuous stirring at room temperature. Samples were collected at regular time intervals throughout the experiment, centrifuged, and analyzed by UV-vis spectroscopy to monitor dye removal. The overall duration of each experimental run was therefore 80 min.

2.8.2. Combined adsorption, photocatalysis, and advanced oxidation processes (AOPs). The combined adsorption–photocatalysis–AOP experiments were conducted following the same two-step protocol described above. After the initial 30 min dark adsorption period and immediately prior to UV irradiation, hydrogen peroxide (H_2O_2) was introduced into the suspension as an external oxidizing agent. Photocatalytic degradation was then carried out under identical UV irradiation conditions for 50 min. Additional H_2O_2 injections were performed at predetermined time intervals during the irradiation phase, as detailed previously.

2.9. Quantification of adsorption and removal efficiency

The adsorption performance of a material refers to its ability to capture and retain pollutants under specific conditions, measured by the equilibrium adsorption parameter q. This parameter represents the amount of pollutant absorbed per unit mass of the adsorbent. The formulas below were used to compute the amount of CV adsorbed onto the biosorbents at equilibrium (q_e, mg g^{-1}) or at a specific time interval (q_t, mg g^{-1}) (eqn (2) and (3)):

$$q_e = (C_0 - C_e)/m \times V \quad (2)$$

$$q_t = (C_0 - C_t)/m \times V \quad (3)$$

where, C_0 is adsorbate initial concentration at $t = 0$ (mg L^{-1}), C_e is adsorbate concentration at equilibrium (mg L^{-1}), C_t denotes concentration at a specific time t (mg L^{-1}), V is the solution volume (L), and (m) is adsorbent weight (g).

2.10. Dye removal efficiency

Dye removal efficiency refers to the proportion of dye adsorbed at a given time relative to its initial concentration in the solution. The percentage of dye elimination is assessed as follows (eqn (4)):

$$\%\ \text{Removal} = (C_0 - C_e)/C_0 \times 100 \quad (4)$$

2.11. Point of zero charge (pH_{pzc})

The surface charge behavior during removal processes is particularly important when electrostatic interactions play a critical role, as typically observed in composite materials. To investigate this, the pH_{pzc} of TiO_2/ZnO-CaAlg composites beads was evaluated.[46] In this process, 0.15 g of the composite material was added to 50 mL of a 0.01 M NaCl solution. The initial pH of each solution was adjusted within the range of 1 to 10 using 1 M HCl or NaOH. The samples were magnetically stirred at 250 rpm for 24 hours at room temperature. Afterward, the final pH values were measured and compared to the initial values to determine the pH_{pzc}.[47] The pH_{pzc} corresponds to the pH at which the final and initial pH values are equal, indicating that the material has no net surface charge.[48]

2.12. Assessment of microbial toxicity

The microbial toxicity of CV dye was assessed both before and after its removal using three bacterial strains from the American Type Culture Collection (ATCC): *Staphylococcus aureus* ATCC®6538 (Gram-positive), *Pseudomonas aeruginosa* ATCC®27853 (Gram-negative), and *Escherichia coli* ATCC®25922. These strains were obtained from the Algerian Pasteur Institute. Toxicity testing, including the evaluation of the dye and its byproducts, was conducted using the agar diffusion method. Each bacterial strain cultivated in nutrient broth at 37 °C for 18 h. The inoculum was then prepared by standardizing the bacterial suspensions to concentrations of 10^{-5} and 10^{-6} CFU mL^{-1}. The suspensions were equally distributed on the surfaces of Muller-Hinton agar plates. Blank and serially prepared disks were put on agar, each impregnated with 30 μL of a 100 mg L^{-1} CV dye solution (both before and after removal *via* the TiO_2/ZnO-CaAlg composite), were placed on the agar. The plates were incubated at 37 °C for 24 hours.

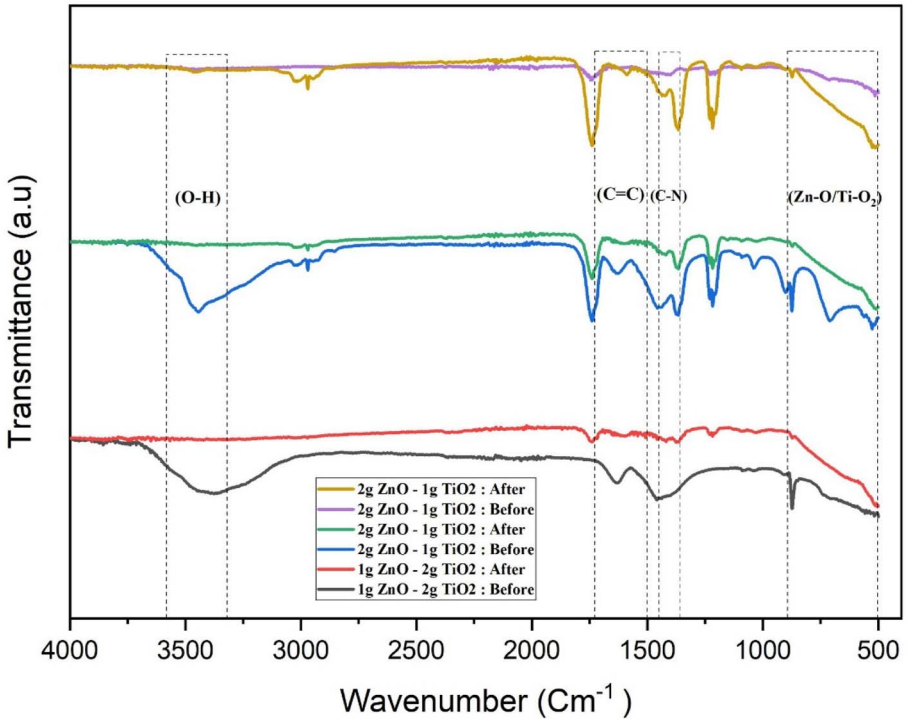

Fig. 3 FTIR spectra of TiO_2/ZnO-CaAlg composites beads before and after CV adsorption.

After incubation, inhibition zones surrounding the disks were evaluated to assess microbial growth inhibition, providing an estimate of microbial toxicity.[49]

3. Results and discussion

3.1. Structural characterization

3.1.1. FT-IR analysis. The FT-IR spectra of the ZnO/TiO_2-CaAlg composite beads recorded before and after CV adsorption (Fig. 3) reveal the characteristic vibrational features of both the alginate matrix and the embedded metal oxides. Prior to adsorption, the broad absorption band centered at approximately 3400 cm^{-1} is attributed to O–H stretching vibrations of hydroxyl groups, while the bands in the 1600–1400 cm^{-1} region correspond to the asymmetric and symmetric stretching modes of carboxylate groups, confirming the presence of alginate functional groups.[43] In addition, metal–oxygen lattice vibrations associated with TiO_2 and ZnO are observed in the low-frequency region between 400–700 cm^{-1} region.[50]

Following CV adsorption, a marked attenuation of the carboxylate bands at ~1600 and ~1400 cm^{-1} is observed, indicating the direct involvement of $-COO^-$ groups in dye binding indicative of dye binding *via* electrostatic forces, while modifications in the broad O–H stretching region around 3400 cm^{-1} region suggest the formation of hydrogen bonds between alginate hydroxyl groups and CV molecules.[47] The appearance or intensification of bands in the 1500–1600 cm^{-1}, characteristic of the aromatic rings of CV, further confirms the successful adsorption of the dye onto the composite beads. Notably, differences in spectral evolution among composites with varying TiO_2/ZnO ratios underscore the role of the metal oxides in the adsorption process. More pronounced spectral changes are observed for the 2 : 1 TiO_2/ZnO composite, whereas the 2 : 2 formulation exhibits weaker variations, which may be attributed to partial saturation or reduced accessibility of active adsorption sites. Overall, the FT-IR analysis demonstrates that CV removal proceeds through a combination of electrostatic attraction and hydrogen-bonding interactions mediated by alginate functional groups, with additional contributions arising from the incorporated metal oxides.

3.1.2. X-ray diffraction (XRD) analysis. The XRD patterns of the TiO_2/ZnO-CaAlg composites beads recorded before and after adsorption and photocatalytic experiments are shown in Fig. 4. For all investigated compositions (2 g TiO_2–1 g ZnO, 1 g TiO_2–2 g ZnO, and 2 g TiO_2–2 g ZnO), the diffraction patterns obtained prior to treatment display the characteristic reflections of anatase TiO_2 and wurtzite ZnO, confirming the successful incorporation of both metal oxides within the alginate matrix.[51,52]

Following adsorption and photocatalytic treatment, the main diffraction peaks associated with TiO_2 and ZnO remain clearly visible, with no emergence of additional phases or loss of characteristic reflections characteristic reflections. This observation indicates that the bulk crystalline structure and phase composition of the composites are maintained throughout the experimental processes. The minor variations in peak intensities observed after treatment are attributed to surface-related effects, such as dye adsorption, the presence of the alginate matrix, and inherent experimental variability, rather than to any crystallographic transformation or amorphization[53–55]

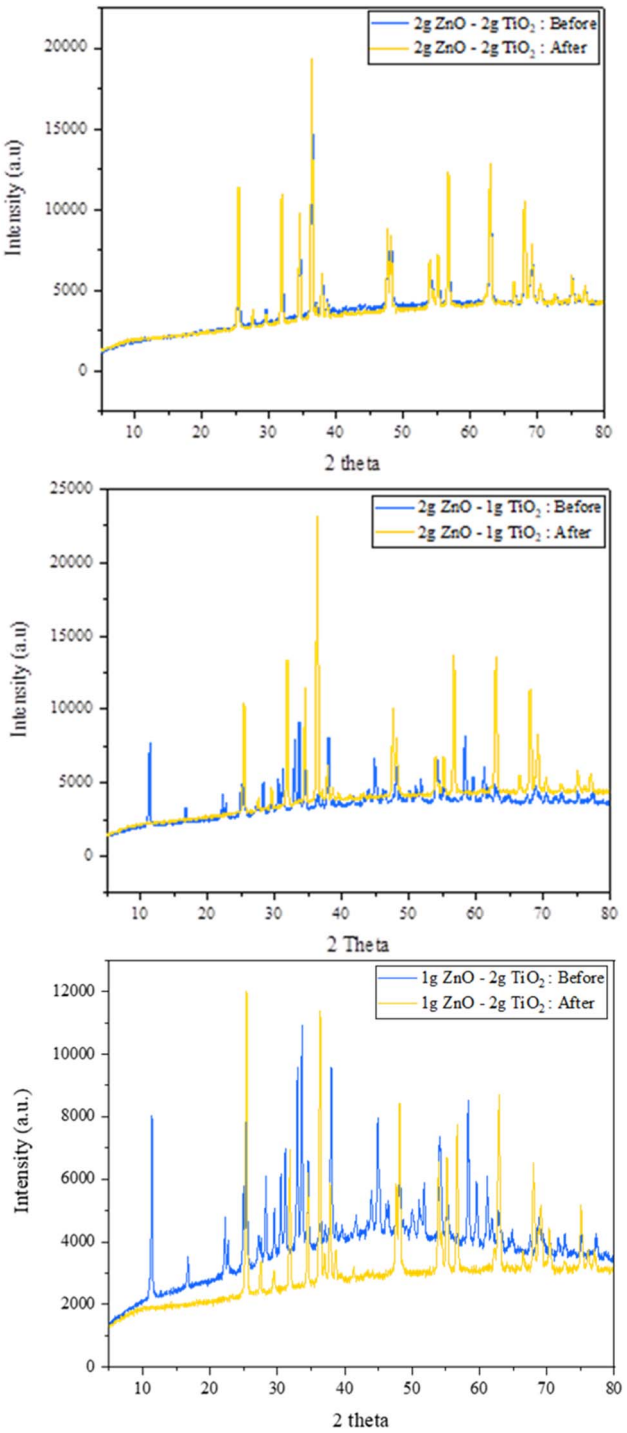

Fig. 4 XRD analysis of TiO_2/ZnO-CaAlg composites beads before and after adsorption and photocatalysis.

Overall, the XRD results confirm the excellent phase stability and structural integrity of the TiO_2/ZnO-CaAlg composites beads before and after use, supporting their robustness and suitability for repeated adsorption–photocatalysis applications.[56,57]

3.1.3. SEM/EDS analysis. SEM/EDS analyses of TiO_2/ZnO-CaAlg composite beads with varying oxide ratios (2 : 2, 2 : 1, and 1 : 2) before and after CV removal is shown in Fig. 5. Prior to adsorption, SEM micrographs reveal distinct surface morphologies as a function of the TiO_2/ZnO ratio. The 2 : 2 composite exhibits a relatively homogeneous porous surface, indicative of uniform oxide dispersion within the alginate matrix. In contrast, the 2 : 1 composite displays porous agglomerates interspersed with elongated, ZnO-like crystalline structures, which are expected to increase surface roughness and enhance the density of accessible adsorption sites.[58] Conversely, the 1 : 2 composite is characterized by the predominance of well-defined TiO_2 crystalline domains, a morphology more conducive to photocatalytic processes.

Following CV adsorption, all composites display partial pore blockage and surface coverage, providing clear evidence of effective dye accumulation on the bead surfaces.[54,59]

EDS analysis prior to adsorption confirms the presence of carbon and oxygen originating from the alginate framework, calcium associated with Ca-alginate ionic crosslinking, and zinc and titanium corresponding to the incorporated metal oxides. The relative intensities of Zn and Ti signals closely match the nominal synthesis ratios, while trace amounts of chlorine are detected before treatment.[60,61] After CV removal, a pronounced increase in carbon content is observed, corroborating the immobilization of the dye on the composite surface. Minor variations in the Zn and Ti signal intensities are attributed to surface masking by adsorbed CV molecules rather than to metal oxide dissolution or leaching.[60,61] Moreover, the persistence of calcium signals and the absence of chlorine after adsorption highlight the structural integrity and chemical stability of the Ca-alginate matrix throughout the treatment process, in good agreement with previously reported findings.[40]

3.2. Optimization of operating conditions

3.2.1. Initial concentration and contact time effect. The influence of contact time on CV removal by ZnO/TiO_2-CaAlg composite beads was investigated to determine the equilibrium time and identify optimal operating conditions. Kinetic experiments were conducted at the natural pH of the solution using initial CV concentrations of 10, 25, and 50 mg L^{-1} and catalyst dosages of 0.05, 0.10, and 0.20 g, in order to evaluate their effects on degradation kinetics and to elucidate the underlying removal mechanism (Fig. S1).

The experiments demonstrated that equilibrium was reached rapidly, within approximately 60 minutes. The CV removal process followed a triphasic kinetic profile. The first stage, occurring during the initial 40 minutes, is characterized by a rapid degradation rate, attributed to the efficient interaction of CV molecules with a large number of readily accessible active sites on the composite surface, governed predominantly by external mass transfer phenomena.[62,63] This is followed by a second, slower stage between 40 and 60 min, during which the degradation rate progressively decreases as surface active sites become increasingly occupied. Finally, a plateau region is observed between 60 and 90 minutes, indicating saturation of the catalyst surface and the establishment of adsorption–degradation equilibrium.

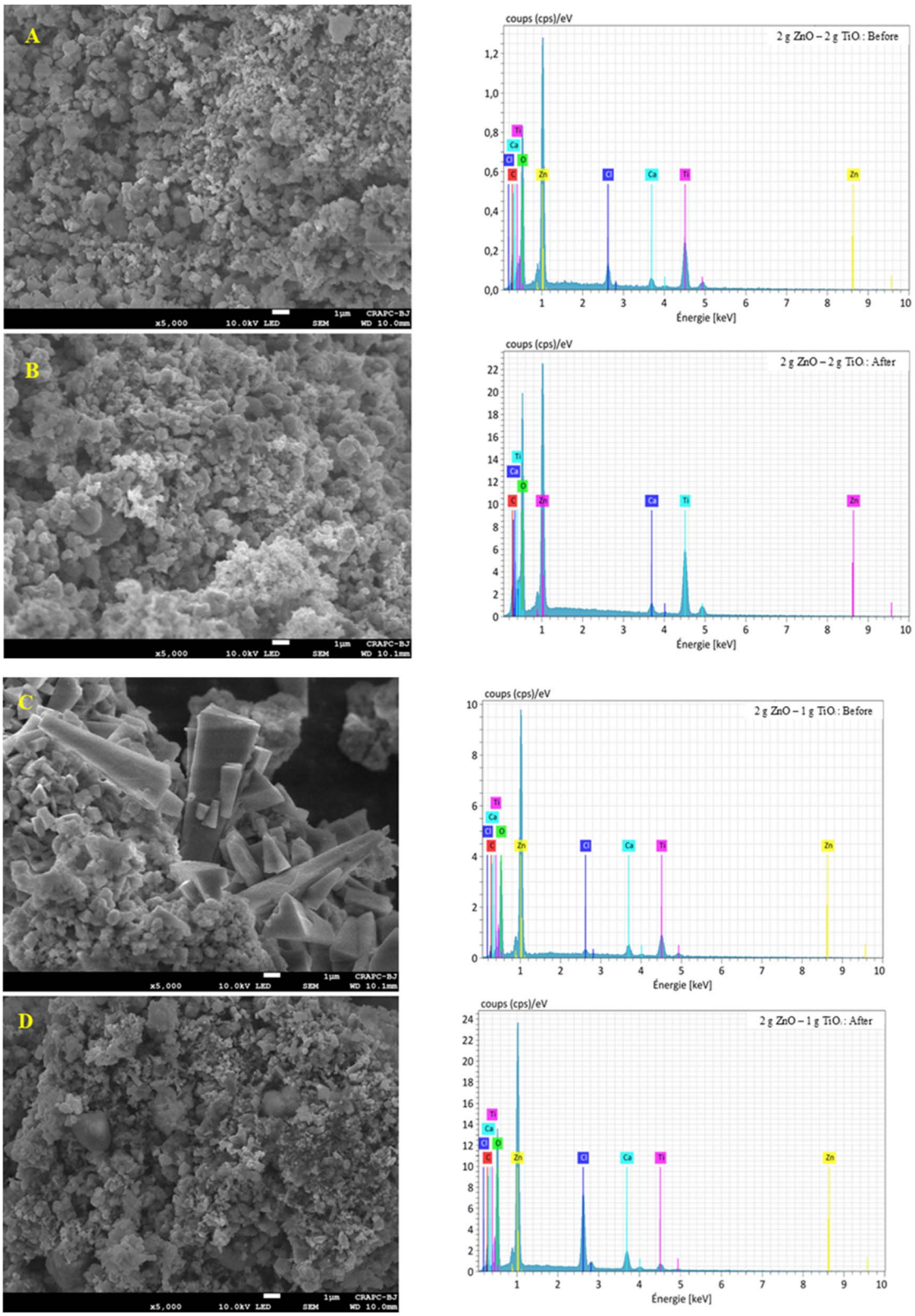

Fig. 5 SEM and EDS analyses of TiO_2/ZnO–CaAlg composite beads with different TiO_2/ZnO ratios before and after CV removal: (A) SEM images before adsorption, (B) SEM images after adsorption, (C) EDS spectra before adsorption, and (D) EDS spectra after adsorption.

These results highlight the critical influence of nanoparticles surface characteristics and textural properties in governing CV degradation efficiency. Among the investigated materials, the composite containing 2 g ZnO and 1 g TiO_2 exhibited superior performance, as evidenced by the lowest normalized concentration (C/C_0) values. Fig. 6 illustrates the temporal evolution of

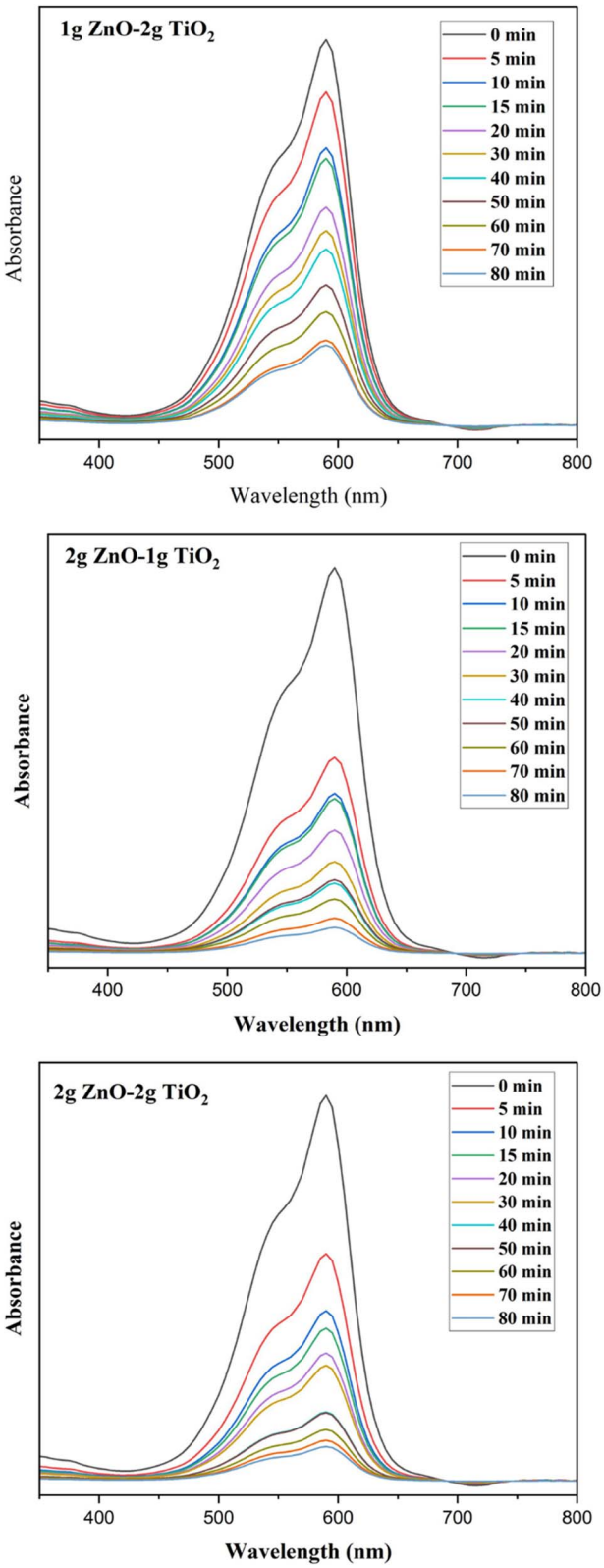

Fig. 6 UV-vis spectral changes of CV solution as a function of degradation time using ZnO/TiO_2-CaAlg composite beads.

the UV-vis spectra of a CV solution (10 mg L^{-1}) before and during degradation in the presence of ZnO/TiO_2-CaAlg composite beads. The initial spectrum exhibits a distinct absorption band in the visible region at λ_{max} = 590 nm, characteristic of CV dye. As the reaction time increases, this band progressively decreases and eventually disappears, indicating effective dye degradation due to the action of reactive oxidative species.[64]

3.2.2. Effect of catalyst mass. Catalyst mass is a critical parameter governing both adsorption efficiency and photocatalytic degradation performance. To evaluate its influence, experiments were conducted using different catalyst dosages. The results show that a catalyst mass of 0.10 g of the 2g ZnO/1g TiO_2-CaAlg composite beads produced the most pronounced reduction in the normalized concentration (C/C_0), reaching a minimum value within approximately 50 min and continuing to decrease thereafter (Fig. S2). This behavior indicates more efficient utilization of active sites and enhanced generation of reactive species, thereby identifying 0.10 g as the optimal catalyst dosage for effective CV degradation under the investigated conditions.

3.2.3. Effect of hydrogen peroxide (H_2O_2) volume on CV dye degradation. Hydrogen peroxide (H_2O_2) serves as an important source of hydroxyl radicals ($OH^{\bullet}$). The effect of varying H_2O_2 volumes on CV dye degradation was investigated using 2g ZnO/1g TiO_2-CaAlg composite beads as the catalyst, with H_2O_2 volumes of 1 μl, 1.5 μl, and 2 μl. As shown in Fig. S2, the addition of H_2O_2 markedly enhanced CV removal, leading to a rapid decrease in the C/C_0 ratio within the first 20–30 minutes. Among the evaluated conditions, an H_2O_2 volume of 1.5 μL yielded the lowest C/C_0 values after 70 min of reaction, indicating the most efficient degradation performance.

The proposed photocatalytic degradation mechanism, involving the generation of reactive oxygen species through UV/H_2O_2-assisted processes, is consistent with mechanisms widely reported in the literature. However, it should be emphasized that this mechanism represents a plausible interpretation of the observed trends rather than a pathway directly confirmed by experimental radical identification studies.[65]

3.2.4. Effect of initial solution pH. The solution pH is a critical parameter influencing both the adsorption behavior and degradation efficiency of CV dye.[66] In this study, the effect of initial pH on CV degradation was investigated using 2 g ZnO/1 g TiO_2-CaAlg composite beads, as illustrated in Fig. S2.

The results demonstrate a dependence of CV removal efficiency on solution pH. The most pronounced decrease in the normalized concentration (C/C_0), corresponding to an approximate removal efficiency of 95%, was achieved at pH 8. In contrast, higher C/C_0 values were observed at pH 2, 4, and 10, indicating reduced degradation performance under strongly acidic or highly alkaline conditions. These findings suggest that a mildly alkaline environment provides optimal conditions for CV degradation.

3.3. Point of zero charge (pH_{pzc})

The point of zero charge (pH_pzc) corresponds to the pH at which the net surface charge of a solid is zero.[67] To determine the pH_{pzc}, a 50 ml NaCl solution was prepared in sealed tubes, with the pH adjusted between 1 and 10 using sodium hydroxide and

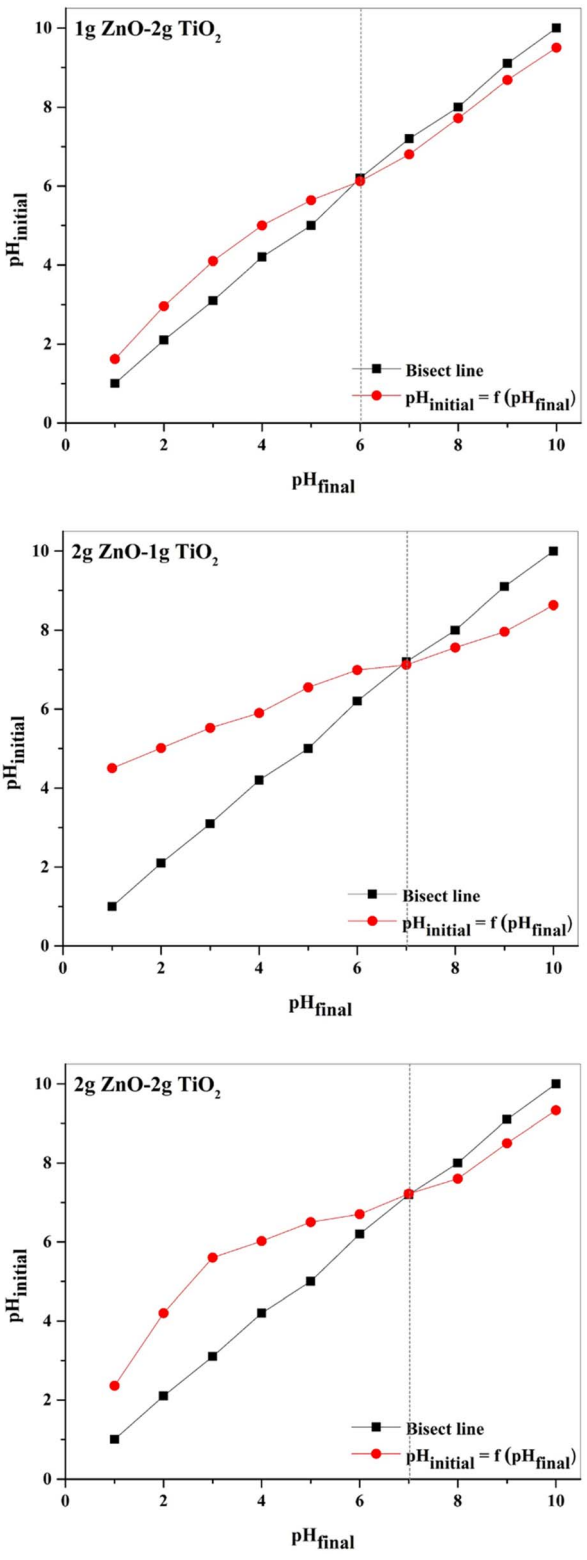

Fig. 7 Zero charge point (pH_{pzc}) of ZnO/TiO_2-CaAlg composite beads.

hydrochloric acid. A 0.05 g sample of ZnO/TiO_2-CaAlg composite beads was then added to each NaCl solution at different pH levels. After 24 hours of stirring, the final pH was measured. A plot was created with the final pH *versus* initial pH, and the point where the plot intersects the line where pH (final) = pH (initial) represents the pH_{pzc} of the material. This value is important as it affects the surface charge of the catalysts.[63] Fig. 7 presents the pH at the point of zero charge (pH_{pzc}) of the ZnO/TiO_2-CaAlg composite beads. The pH_{pzc} of the composite containing 1 g ZnO and 2 g TiO_2 is approximately 6, whereas the composites with 2 g ZnO/1 g TiO_2 and 2 g ZnO/2 g TiO_2 exhibit pH_{pzc} values close to 7. At solution pH values exceeding the pH_{pzc}, the surface of the composite beads becomes negatively charged, favoring the adsorption of cationic species such as crystal violet through electrostatic attraction. In contrast, at pH values below the pH_{pzc}, the surface acquires a net positive charge, leading to electrostatic repulsion with cationic dye molecules and consequently lower removal efficiency. These results indicate that electrostatic interactions play an important role in the adsorption process, particularly under neutral to slightly alkaline conditions, although they may act in conjunction with other surface interactions on heterogeneous adsorption sites.[68]

3.4. Effect of temperature

Temperature is a key parameter influencing photocatalytic degradation processes, as it affects dye solubility, molecular mobility, and the physicochemical properties of the catalyst surface.[69] An increase in temperature generally enhances molecular diffusion by lowering solution viscosity, thereby facilitating mass transfer and improving degradation efficiency.[70] In this study, the effect of temperature on the photocatalytic degradation of CV using ZnO/TiO_2-CaAlg composite beads was investigated over a temperature range of 20–60 °C (Fig. S2).

A systematic decrease in the C/C_0 ratio was observed with increasing temperature, indicating enhanced dye degradation and suggesting that the process is endothermic in nature.[71] The improved performance at higher temperatures can be attributed to increased molecular mobility of CV molecules and strengthened interactions with the active sites on the ZnO/TiO_2-CaAlg surface, which collectively promote adsorption and subsequent photocatalytic reactions.

At 60 °C, the lowest C/C_0 values were obtained for the 1g ZnO/2g TiO_2, 2g ZnO/1g TiO_2, and 2 g ZnO/2g TiO_2 composites beads, confirming the beneficial effect of increased temperature on photocatalytic activity across all investigated compositions.

3.5. Kinetic modeling of CV dye photodegradation

This study investigated the photodegradation kinetics of CV dye using the synthesized ZnO/TiO_2-CaAlg composites beads, employing both pseudo-first-order (Langmuir–Hinshelwood) and pseudo-second-order models to assess photocatalytic performance.[72] In the pseudo-first-order kinetic model, the relationship between ln (C_0/C_t) and time (t) is considered, whereas in the pseudo-second-order model, the relationship between $(1/C_t - 1/C_0)$ and time (t) is used. These equations are presented in Table S1.

The apparent rate constants were obtained from the slopes of the kinetic plots provided in Table S1, and the calculated

Table 1 Kinetic model parameters and correlation coefficients for CV dye removal by the prepared nanocomposites[a]

	Pseudo-first-order		Pseudo-second-order	
Composite catalysts	k_1 (min^{-1})	R^2	k_2 (L mg^{-1} min^{-1})	R^2
1g ZnO-2g TiO_2	0.0192	0.9866	0.004	0.9531
2g ZnO-1g TiO_2	0.0249	0.9799	0.007	0.9102
2g ZnO-2g TiO_2	0.0251	0.9808	0.008	0.9619

[a] kinetic parameters were obtained from the overall removal process following sequential adsorption and photocatalysis steps.

values are summarized in Table 1. For ZnO/TiO_2-CaAlg composites beads, the rate constants increase from 0.0192 min^{-1} and 0.004 L mg^{-1} min^{-1} (1g ZnO-2g TiO_2) to 0.0249 min^{-1} and 0.007 L mg^{-1} min^{-1} (2g ZnO-1g TiO_2), reaching 0.0251 min^{-1} and 0.008 L mg^{-1} min^{-1} for 2g ZnO-2g TiO_2. This progressive enhancement reflects improved photocatalytic activity, likely due to more efficient charge separation and an increased density of active sites in the optimized nanocomposite. The results demonstrate that the photodegradation of CV follows both pseudo-first-order and pseudo-second-order kinetics, with correlation coefficients exceeding 0.9.[73]

3.6. Adsorption and photodegradation isotherm modeling of CV dye

Experimental data were analyzed using the Langmuir and Freundlich isotherm models to describe the adsorption behavior and elucidate interactions between CV dye molecules and the catalyst surface.[74,75] Adsorption isotherms of CV dye at varying initial dye concentrations are presented in Fig. S3 and were fitted using the non-linear Langmuir and Freundlich models (Table S1). The corresponding isotherm parameters for ZnO/TiO_2-CaAlg composite beads are summarized in Table 2. High q_{max} or K_F values indicate strong adsorption capacity, while $1/n$ values between 0 and 1 confirm favorable adsorption.[76]

As shown in Table 2, both Langmuir and Freundlich models exhibit high correlation coefficients ($R^2 \geq 0.90$), indicating good agreement with the experimental data. The Langmuir model provides an excellent fit for the 2g ZnO/2g TiO_2 ($R^2 = 0.99$) and 2 g ZnO/1g TiO_2 ($R^2 = 0.96$) composites suggesting that CV adsorption predominantly occurs as a monolayer on energetically uniform surface sites.[77] Based on the Langmuir model, 1g ZnO/2g TiO_2 shows the highest adsorption capacity (826.57 mg g^{-1}), followed by 2g ZnO/2g TiO_2 (612.95 mg g^{-1}) and 2g ZnO/1g TiO_2 (263.78 mg g^{-1}). The Freundlich parameter $1/n$ values ($0 < 1/n < 1$) further confirm favorable adsorption on heterogeneous surfaces.

3.7. Thermodynamic analysis of the process

Thermodynamic parameters, including Gibbs free energy (ΔG), enthalpy (ΔH), and entropy (ΔS), were evaluated to assess the spontaneity and energetic feasibility of CV adsorption on ZnO/TiO_2-CaAlg composite beads. The equations used for these calculations are provided in Table S1.[78]

The thermodynamic parameters were obtained from the slope and intercept of the ln (K_d) *versus* $1/T$ plot (Fig. S4) and are

Table 3 Thermodynamic parameters for CV photocatalytic degradation on ZnO/TiO_2-CaAlg composite beads

CaAlg nanoparticles	T (°K)	$\Delta G°$ (kJ mol^{-1})	$\Delta H°$ (kJ mol^{-1})	$\Delta S°$ (J mol^{-1} K^{-1})
1g ZnO/2g TiO_2	293	−0.66	14.29	51.93
	303	−1.65		
	313	−2.52		
	333	−2.75		
2g ZnO/1g TiO_2	293	−3.80	18.10	75.54
	303	−5.18		
	313	−5.99		
	333	−6.87		
2g ZnO/2g TiO_2	293	−2.42	15.62	61.61
	303	−2.94		
	313	−4.06		
	333	−4.74		

Table 2 Adsorption isotherm model parameters obtained from experimental data

		Parameters		
Isotherm models	CaAlg nanoparticles	q_{max} (mg g^{-1})	K_L(L mg^{-1})	R^2
Langmuir	1g ZnO/2g TiO_2	826.57	0.030	0.89
	2g ZnO/1g TiO_2	263.78	0.15	0.96
	2g ZnO/2g TiO_2	612.95	0.020	0.99
		Parameters		
Isotherm models	CaAlg nanoparticles	K_F (mg g^{-1})	$1/n$	R^2
Freundlich	1g ZnO/2g TiO_2	26.46	0.87	0.88
	2g ZnO/2g TiO_2	42.43	0.59	0.90
	2g ZnO/2g TiO_2	14.92	0.84	0.98

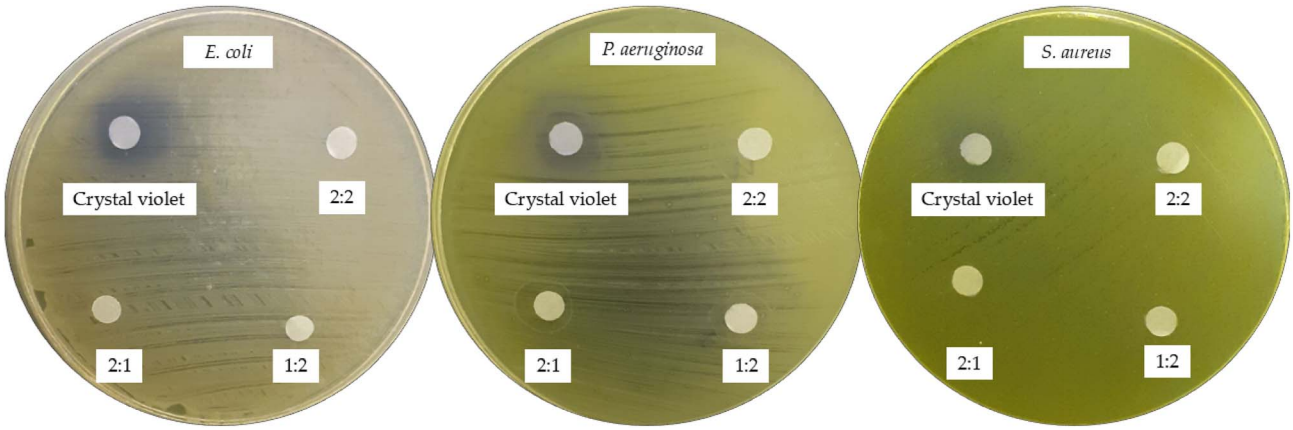

Fig. 8 Microbial toxicity *of E. coli*,*P. aeruginosa*, and *S. aureus* exposed to crystal violet and TiO_2/ZnO-CaAlg composite-treated solutions.

summarized in Table 3. The negative ΔG values over the studied temperature range confirm the spontaneous nature of the process, while their decrease with increasing temperature indicates enhanced spontaneity at higher temperatures. The positive ΔH value reveals that the adsorption process is endothermic.[79] Furthermore, the positive ΔS value indicates an increase in randomness at the solid–liquid interface during adsorption, reflecting enhanced disorder as dye molecules interact with the nanoparticle surface.

3.8. Evaluation of microbial toxicity and detoxification of CV dye using ZnO/TiO_2-CaAlg composite beads

The microbial toxicity test results (Fig. 8) showed that the crystal violet stock solution (100 mg L^{-1}) produced clear inhibition zones, ranging from 12 mm for *Staphylococcus aureus* to 14 mm for *Pseudomonas aeruginosa* and 20 mm for *Escherichia coli*, confirming the acute toxicity of crystal violet toward the tested bacterial strains.

In contrast, solutions treated with TiO_2/ZnO-CaAlg composites beads prepared at varying oxide ratios (2 g ZnO–2 g TiO_2, 2 g ZnO–1 g TiO_2, and 1 g ZnO–2 g TiO_2) exhibited no detectable inhibition zones for any of the tested bacteria. This result indicates a substantial reduction of microbial toxicity after treatment.

It is important to emphasize that the disappearance of inhibition zones reflects detoxification, defined here as the loss of acute antimicrobial activity toward the tested microorganisms. This outcome does not necessarily imply complete mineralization of crystal violet, as adsorbed dye molecules or transformation intermediates may still be present at non-toxic concentrations. Nevertheless, the microbial assay provides relevant evidence that the treated effluents no longer exert harmful biological effects under the tested conditions, highlighting the potential of TiO_2/ZnO-CaAlg composites for detoxification-oriented wastewater treatment applications.

3.9. Comparative assessment of CV adsorption efficiency

The adsorption performance of the ZnO/TiO_2-CaAlg composite beads prepared in this study was evaluated and benchmarked against various alginate-based composites reported in the

Table 4 Comparison of CV adsorption capacities (q_{max}) of ZnO/TiO_2-CaAlg composite beads with similar alginate-based composites reported in the literature

Materials used	Composition/ratio	Pollutant	q_{max} (mg g^{-1})	Material type	Ref.
ZnO/TiO_2-CaAlg	1 g ZnO/2 g TiO_2	Crystal violet	826.57	Composite beads	This work
ZnO/TiO_2-CaAlg	2 g ZnO/2 g TiO_2	Crystal violet	612.95	Composite beads	This work
ZnO/TiO_2-CaAlg	2 g ZnO/1 g TiO_2	Crystal violet	263.78	Composite beads	This work
Bentonite–alginate composite	Bentonite/alginate	Crystal violet	601.93	Composite beads	80
Alginate/acid-activated bentonite	Alginate/AAB	Crystal violet	582.4	Composite beads	81
Bentonite/alginate	Activated bentonite + alginate	Crystal violet	546	Composite beads	82
Alginate/Pectin nanocomposite	Alginate/pectin	Crystal violet	619.22	Biopolymer nanocomposite	83
Alginate/gelatin/MMT	Alginate/gelatin/montmorillonite	Crystal violet	1000.0	Ternary composite beads	84
Ionic-liquid alginate hydrogel	IL-crosslinked alginate	Crystal violet	405.0	Functional hydrogel	85
Alginate–whey	Alginate/whey	Crystal violet	220.0	Biopolymer composite	86
Alg@AgNPs	Alginate/Ag nanoparticles	Crystal violet	186.93	Bionanocomposite	87
Alg-Cst/Kal	Alginate/chitosan/kaolinite	Crystal violet	169.49	Bio-nanocomposite	88
Alginate/GO hydrogel	Alginate/acrylamide/GO	Crystal violet	100.30	Hydrogel nanocomposite	89
Alginate/ZnO/GO	Grafted alginate/ZnO/GO	Crystal violet	13.85	Photocatalytic composite	90
Alginate beads + sawdust	Alginate/Cedrus deodara	Crystal violet	4.80	Beads/biosorbent	91
Guar gum/alginate hydrogel	Guar gum/alginate	Crystal violet	3.25	Hydrogel	92

literature (Table 4). Among the three compositions tested, the 1 g ZnO/2 g TiO_2 beads exhibited the highest maximum adsorption capacity toward CV, with a q_{max} of 826.57 mg g^{-1}, followed by 2 g ZnO/2 g TiO_2 (612.95 mg g^{-1}) and 2 g ZnO/1 g TiO_2 (263.78 mg g^{-1}). These adsorption capacities are comparable to, and, in some cases, surpass, those reported for other alginate-based composite beads, hydrogels, and nanocomposites, including bentonite–alginate (601.93 mg g^{-1}), alginate/acid-activated bentonite (582.4 mg g^{-1}), and alginate/pectin nanocomposites (619.22 mg g^{-1}). Notably, only alginate/gelatin/montmorillonite ternary composite beads achieved a higher q_{max} (1000 mg g^{-1}), highlighting the excellent performance of the ZnO/TiO_2-CaAlg beads within the context of alginate-based systems. These results indicate that adjusting the ZnO/TiO_2 ratio has a significant impact on adsorption efficiency, with higher TiO_2 content promoting enhanced CV adsorption.

4. Conclusions

This study investigates the challenge of effective wastewater treatment by evaluating the degradation of crystal violet dye using ZnO/TiO_2-CaAlg catalysts. The results highlight the effectiveness of a hybrid approach that combines adsorption and photocatalysis, achieving optimal dye removal under specific conditions, including pH, dye concentration, catalyst dosage, and H_2O_2 volume. In summary, the key conclusions from this work are as follows:

- The ZnO/TiO_2-CaAlg composites beads, especially with a ZnO : TiO_2 ratio of 2 : 1, exhibit a porous structure with abundant active sites, facilitating strong interactions with dye molecules. After adsorption, a notable increase in carbon and oxygen content confirms effective dye adsorption and photocatalysis, with significant coverage of the crystal surfaces.
- XRD analysis shows distinct crystalline phases for ZnO (wurtzite) and TiO_2 (anatase) before adsorption, while a decrease in peak intensity after adsorption indicates structural modifications. The 2 : 1 composite demonstrates the highest efficiency in both adsorption and photocatalysis.
- FTIR analysis reveals the formation of chemical bonds between the dye and the composite, as evidenced by the attenuation of carboxylate and hydroxyl groups after adsorption.
- Antimicrobial tests show that while crystal violet dye inhibits bacterial growth, treatment with the ZnO/TiO_2-CaAlg composites beads eliminates the dye's toxicity, with no residual harmful effects on bacteria.
- The point of zero charge (pH_{pzc}) of the composites varies with the ratio, influencing adsorption behavior, particularly at different solution pH levels. For optimal decolorization, a 0.1 g mass of the 2 : 1 composite achieves 98.5% dye removal efficiency under optimal conditions.

The enhanced performance of ZnO/TiO_2-CaAlg composites stems from the synergistic integration of metal oxide nanoparticles within the alginate matrix, which provides abundant accessible active sites, increased porosity, and optimized surface area. These characteristics collectively enable efficient crystal violet adsorption and effective photocatalytic degradation through improved charge separation and reactive oxygen species generation. Notably, the 2 : 1 ZnO/TiO_2-CaAlg composition exhibits outstanding potential for dye removal and microbial detoxification, highlighting its promise for advanced wastewater treatment applications.

Author contributions

Nesrine Ammouchi: conceptualization; Methodology; investigation; resources; data curation; writing–original draft preparation. Abdallah Zaiter: methodology; formal analysis; resources; Atmane Djermoune: software; resources; visualization. Nawal Bouzenad: conceptualization; methodology; software; formal analysis; investigation; resources; data curation; writing–original draft preparation; visualization. Nada Hamrouche: methodology; formal analysis; investigation; writing–original draft preparation; visualization. Amdjed Abdennouri: formal analysis; investigation; writing–original draft preparation; visualization. Youghourta Belhocine: methodology; validation; writing–review and editing. Najoua Sbei: validation; data curation. Writing–review and editing. Seyfeddine Rahali: validation; investigation; writing–review and editing; Fehmi Boufahja: software, investigation, formal analysis; Tareh H. Taha: validation, writing–review and editing Walid Elfalleh: validation, writing–review and editing; Stefania Garzoli: writing–review and editing, supervision; Hamdi Bendif: writing–review and editing, project administration, supervision; Djihane Slimane Ben Ali : writing–review and editing, supervision.

Conflicts of interest

The authors declare no conflicts of interest.

Data availability

All data supporting the findings of this study are included within the manuscript.

Supplementary information: additional experimental details, electrochemical figures, calibration data, and tables. See DOI: https://doi.org/10.1039/d5ra09465h.

Acknowledgements

This work was supported and funded by the Deanship of Scientific Research at Imam Mohammad Ibn Saud Islamic University (IMSIU) (grant number IMSIU-DDRSP2602).

References

1 T. Islam, Md. R. Repon, T. Islam, Z. Sarwar and M. M. Rahman, Impact of Textile Dyes on Health and Ecosystem: A Review of Structure, Causes, and Potential Solutions, *Environ. Sci. Pollut. Res.*, 2023, **30**(4), 9207–9242, DOI: 10.1007/s11356-022-24398-3.
2 A. Tkaczyk, K. Mitrowska and A. Posyniak, Synthetic Organic Dyes as Contaminants of the Aquatic Environment and Their

Implications for Ecosystems: A Review, *Sci. Total Environ.*, 2020, **717**, 137222, DOI: 10.1016/j.scitotenv.2020.137222.

3 D. Zouied, W. Chettah, M. Khelfaoui, N. Bouzenad, A. Abdennouri, K. Dob, H. Bouhali, K. Derdour, N. Ammouchi and E. Zouaoui, The Use of Arum Italicum Root Extracts for Protection Against Corrosion and Green Synthesis of Silver Nanoparticles: Investigation of Their Photocatalytic and Antimicrobial Properties, *Global NEST J.*, 2024, 1–9, DOI: 10.30955/gnj.06931.

4 J. Singh, P. Gupta and A. Das, Dyes from Textile Industry Wastewater as Emerging Contaminants in Agricultural Fields. in *Sustainable agriculture reviews 50: emerging contaminants in agriculture*, ed. Kumar Singh. V., Singh. R., Lichtfouse. E., Springer International Publishing, Cham, 2021, pp. 109–129, DOI: 10.1007/978-3-030-63249-6_5.

5 K. Dob, D. Zouied, M. Khelfaoui, N. Bouzenad, A. Abdennouri and M. Rouainia, Pulicaria Odora Ethanolic Extract as a Corrosion Inhibitor and Its Eco-Friendly Synthesis of CuO Nanoparticles for Photocatalytic and Microbial Properties, *Chem. Biochem. Eng. Q.*, 2025, **39**(3), 157–166, DOI: 10.15255/CABEQ.2025.2429.

6 M. Ismail, K. Akhtar, M. I. Khan, T. Kamal, M. A. Khan, A. M. Asiri, J. Seo and S. B. Khan, Pollution, Toxicity and Carcinogenicity of Organic Dyes and Their Catalytic Bio-Remediation, *Curr. Pharm. Des.*, 2019, **25**(34), 3645–3663, DOI: 10.2174/1381612825666191021142026.

7 F. Uddin, Environmental Hazard in Textile Dyeing Wastewater from Local Textile Industry, *Cellulose*, 2021, **28**(17), 10715–10739, DOI: 10.1007/s10570-021-04228-4.

8 F. Mashkoor, A. Nasar, I. Inamuddin and A. M. Asiri, Exploring the Reusability of Synthetically Contaminated Wastewater Containing Crystal Violet Dye Using Tectona Grandis Sawdust as a Very Low-Cost Adsorbent, *Sci. Rep.*, 2018, **8**(1), 8314, DOI: 10.1038/s41598-018-26655-3.

9 M. Negri, V. Gonçalves, S. Silva, M. Henriques, J. Azeredo and R. Oliveira, Crystal Violet Staining to Quantify Candida Adhesion to Epithelial Cells, *Br. J. Biomed. Sci.*, 2010, **67**(3), 120–125, DOI: 10.1080/09674845.2010.11730308.

10 S. Mani and R. N. Bharagava, Exposure to Crystal Violet, Its Toxic, Genotoxic and Carcinogenic Effects on Environment and Its Degradation and Detoxification for Environmental Safety, in *Reviews of environmental contamination and toxicology*, ed. de Voogt. W. P., Springer International Publishing, Cham, 2016, vol, 237, pp 71–104, DOI: 10.1007/978-3-319-23573-8_4.

11 R. Al-Tohamy, S. S. Ali, F. Li, K. M. Okasha, Y. A.-G. Mahmoud, T. Elsamahy, H. Jiao, Y. Fu and J. Sun, A Critical Review on the Treatment of Dye-Containing Wastewater: Ecotoxicological and Health Concerns of Textile Dyes and Possible Remediation Approaches for Environmental Safety, *Ecotoxicol. Environ. Saf.*, 2022, **231**, 113160, DOI: 10.1016/j.ecoenv.2021.113160.

12 M. B. Bahrodin, N. S. Zaidi, N. Hussein, M. Sillanpää, D. D. Prasetyo and A. Syafiuddin, Recent Advances on Coagulation-Based Treatment of Wastewater: Transition from Chemical to Natural Coagulant, *Curr. Pollut. Rep.*, 2021, **7**(3), 379–391, DOI: 10.1007/s40726-021-00191-7.

13 C. H. Jones, L. G. Terry, R. S. Summers and S. M. Cook, Environmental Life Cycle Comparison of Conventional and Biological Filtration Alternatives for Drinking Water Treatment, *Environ. Sci.:Water Res. Technol.*, 2018, **4**(10), 1464–1479, DOI: 10.1039/C8EW00272J.

14 G. Crini, E. Lichtfouse, L. D. Wilson and N. Morin-Crini, Conventional and Non-Conventional Adsorbents for Wastewater Treatment, *Environ. Chem. Lett.*, 2019, **17**(1), 195–213, DOI: 10.1007/s10311-018-0786-8.

15 N. Hamrouche, C. Djilani, Y. Belhocine, N. Bouzenad, L. Boudjema Amir, S. Meradi, I. Hamrouche and D. S. B. Ali, Comprehensive Characterization and RSM-Based Optimization of Crystal Violet Adsorption Using SnCl 2 –FeCl 3 and SnCl 2 –ZnCl 2 Activated Pomegranate Peel Biosorbents, *RSC Adv.*, 2026, **16**(5), 4318–4334, DOI: 10.1039/D5RA09290F.

16 D. Ma, H. Yi, C. Lai, X. Liu, X. Huo, Z. An, L. Li, Y. Fu, B. Li, M. Zhang, L. Qin, S. Liu and L. Yang, Critical Review of Advanced Oxidation Processes in Organic Wastewater Treatment, *Chemosphere*, 2021, **275**, 130104, DOI: 10.1016/j.chemosphere.2021.130104.

17 A. Babu Ponnusami, S. Sinha, H. Ashokan, M. V Paul, S. P. Hariharan, J. Arun, K. P. Gopinath, Q. Hoang Le and A. Pugazhendhi, Advanced Oxidation Process (AOP) Combined Biological Process for Wastewater Treatment: A Review on Advancements, Feasibility and Practicability of Combined Techniques, *Environ. Res.*, 2023, **237**, 116944, DOI: 10.1016/j.envres.2023.116944.

18 M. Cheng, G. Zeng, D. Huang, C. Lai, P. Xu, C. Zhang and Y. Liu, Hydroxyl Radicals Based Advanced Oxidation Processes (AOPs) for Remediation of Soils Contaminated with Organic Compounds: A Review, *Chem. Eng. J.*, 2016, **284**, 582–598, DOI: 10.1016/j.cej.2015.09.001.

19 L. Fei, M. Bilal, S. A. Qamar, H. M. Imran, A. Riasat, M. Jahangeer, M. Ghafoor, N. Ali and H. M. N. Iqbal, Nano-Remediation Technologies for the Sustainable Mitigation of Persistent Organic Pollutants, *Environ. Res.*, 2022, **211**, 113060, DOI: 10.1016/j.envres.2022.113060.

20 A. Krishnamurthy, B. Adebayo, T. Gelles, A. Rownaghi and F. Rezaei, Abatement of Gaseous Volatile Organic Compounds: A Process Perspective, *Catal. Today*, 2020, **350**, 100–119, DOI: 10.1016/j.cattod.2019.05.069.

21 S. Horoz, C. Orak and E. Biçer, Green Synthesis of ZnO and Ni-Doped ZnO from Okra Stalks for the Photocatalytic Degradation of Procion Red MX-5B, *Int. J. Phytoremediation*, 2025, **27**(2), 206–214, DOI: 10.1080/15226514.2024.2411248.

22 K. P. Gopinath, N. V. Madhav, A. Krishnan, R. Malolan and G. Rangarajan, Present Applications of Titanium Dioxide for the Photocatalytic Removal of Pollutants from Water: A Review, *J. Environ. Manage.*, 2020, **270**, 110906, DOI: 10.1016/j.jenvman.2020.110906.

23 K. M. Lee, C. W. Lai, K. S. Ngai and J. C. Juan, Recent Developments of Zinc Oxide Based Photocatalyst in Water Treatment Technology: A Review, *Water Res.*, 2016, **88**, 428–448, DOI: 10.1016/j.watres.2015.09.045.

24 R. Bakır, C. Orak and S. Horoz, Enhancing Photocatalytic Degradation of Hazardous Pollutants with Green-Synthesized Catalysts: A Machine Learning Approach, *J. Environ. Manage.*, 2025, **385**, 125695, DOI: 10.1016/j.jenvman.2025.125695.
25 G. Verma, K. Mondal, M. Islam and A. Gupta, Recent Advances in Advanced Micro and Nanomanufacturing for Wastewater Purification, *ACS Appl. Eng. Mater.*, 2024, **2**(2), 262–285, DOI: 10.1021/acsaenm.3c00711.
26 H. Bitter, L. Krause, F. Kirchen, T. Fundneider and S. Lackner, Semi-Crystalline Microplastics in Wastewater Plant Effluents and Removal Efficiencies of Post-Treatment Filtration Systems, *Water Res.:X*, 2022, **17**, 100156, DOI: 10.1016/j.wroa.2022.100156.
27 Y. Ma, X. Wang, Y. Jia, X. Chen, H. Han and C. Li, Titanium Dioxide-Based Nanomaterials for Photocatalytic Fuel Generations, *Chem. Rev.*, 2014, **114**(19), 9987–10043, DOI: 10.1021/cr500008u.
28 S. Mehla, J. Das, D. Jampaiah, S. Periasamy, A. Nafady and S. K. Bhargava, Recent Advances in Preparation Methods for Catalytic Thin Films and Coatings, *Catal. Sci. Technol.*, 2019, **9**(14), 3582–3602, DOI: 10.1039/C9CY00518H.
29 N. Bouzenad, N. Ammouchi, A. Abdennouri, A. Bouzana, H. A. Rudayni, F. Boufahja and H. Bendif, Comprehensive Review of Alginate: Sources, Synthesis, and Application in the Food Packaging Sector, *Ital. J. Food Sci.*, 2025, **37**(4), 1–17.
30 A. Kartik, D. Akhil, D. Lakshmi, K. Panchamoorthy Gopinath, J. Arun, R. Sivaramakrishnan and A. Pugazhendhi, A Critical Review on Production of Biopolymers from Algae Biomass and Their Applications, *Bioresour. Technol.*, 2021, **329**, 124868, DOI: 10.1016/j.biortech.2021.124868.
31 J. Pandey, Biopolymers and Their Application in Wastewater Treatment, In*Emerging Eco-Friendly Green Technologies for Wastewater Treatment*, Bharagava, R. N., ed. Springer, Singapore, 2020, pp. 245–266. doi: DOI: 10.1007/978-981-15-1390-9_11.
32 I. Donati and B. E. Christensen, Alginate-Metal Cation Interactions: Macromolecular Approach, *Carbohydr. Polym.*, 2023, **321**, 121280, DOI: 10.1016/j.carbpol.2023.121280.
33 V. S. Kosera, T. M. Cruz, E. S. Chaves and E. R. L. Tiburtius, Triclosan Degradation by Heterogeneous Photocatalysis Using ZnO Immobilized in Biopolymer as Catalyst, *J. Photochem. Photobiol. Chem.*, 2017, **344**, 184–191, DOI: 10.1016/j.jphotochem.2017.05.014.
34 W. Boultif, C. Dehchar, Y. Belhocine, E. Zouaoui, S. Rahali, S. E. Zouari, N. Sbei and M. Seydou, Chitosan and Metal Oxide Functionalized Chitosan as Efficient Sensors for Lead (II) Detection in Wastewater, *Separations*, 2023, **10**(9), 479, DOI: 10.3390/separations10090479.
35 F. Z. Gharbi, N. Bougdah, Y. Belhocine, N. Sbei, S. Rahali, M. Damous and M. Seydou, Green and Fast Extraction of Chitin from Waste Shrimp Shells: Characterization and Application in the Removal of Congo Red Dye, *Separations*, 2023, **10**(12), 599, DOI: 10.3390/separations10120599.
36 E. Colombo, W. Li, S. K. Bhangu and M. Ashokkumar, Chitosan Microspheres as a Template for TiO2 and ZnO Microparticles: Studies on Mechanism, Functionalization and Applications in Photocatalysis and H2S Removal, *RSC Adv.*, 2017, **7**(31), 19373–19383, DOI: 10.1039/C7RA01227F.
37 P. Dhiman, G. Rana, A. Kumar, G. Sharma, D.-V. N. Vo and Mu. Naushad, ZnO-Based Heterostructures as Photocatalysts for Hydrogen Generation and Depollution: A Review, *Environ. Chem. Lett.*, 2022, **20**(2), 1047–1081, DOI: 10.1007/s10311-021-01361-1.
38 Li Xiao-fang, R. Li and X. Feng, Efficient Adsorption and Photocatalytic Degradation of Organic Pollutant by Ag3PO4/ZnO/Chitosan–Biochar Composites, *Russ. J. Inorg. Chem.*, 2023, **68**(10), 1386–1398, DOI: 10.1134/S0036023623601307.
39 A. Gunasekaran, A. K. Rajamani, C. Masilamani, I. Chinnappan, U. Ramamoorthy and K. Kaviyarasu, Synthesis and Characterization of ZnO Doped TiO2 Nanocomposites for Their Potential Photocatalytic and Antimicrobial Applications, *Catalysts*, 2023, **13**(2), 215, DOI: 10.3390/catal13020215.
40 N. Bai, X. Liu, Z. Li, X. Ke, K. Zhang and Q. Wu, High-Efficiency TiO2/ZnO Nanocomposites Photocatalysts by Sol–Gel and Hydrothermal Methods, *J. Sol-Gel Sci. Technol.*, 2021, **99**(1), 92–100, DOI: 10.1007/s10971-021-05552-8.
41 T. Wijesekara and B. Xu, New Insights into Sources, Bioavailability, Health-Promoting Effects, and Applications of Chitin and Chitosan, *J. Agric. Food Chem.*, 2024, **72**(31), 17138–17152, DOI: 10.1021/acs.jafc.4c02162.
42 A. Silva, L. Cassani, M. Carpena, C. Lourenço-Lopes, C. Grosso, F. Chamorro, P. García-Pérez, A. Carvalho, V. F. Domingues, M. F. Barroso, J. Simal-Gandara and M. A. Prieto, Exploring the Potential of Invasive Species Sargassum Muticum: Microwave-Assisted Extraction Optimization and Bioactivity Profiling, *Mar. Drugs*, 2024, **22**(8), 352, DOI: 10.3390/md22080352.
43 N. Bouzenad, N. Ammouchi, N. Chaib, M. Messaoudi, W. Bousabaa, C. Bensouici, B. Sawicka, M. Atanassova, S. F. Ahmad and W. Zahnit, Exploring Bioactive Components and Assessing Antioxidant and Antibacterial Activities in Five Seaweed Extracts from the Northeastern Coast of Algeria, *Mar. Drugs*, 2024, **22**(6), 273, DOI: 10.3390/md22060273.
44 M. R. Torres, A. P. A. Sousa, E. A. T. Silva Filho, D. F. Melo, J. P. A. Feitosa, R. C. M. de Paula and M. G. S. Lima, Extraction and Physicochemical Characterization of *Sargassum Vulgare* Alginate from Brazil, *Carbohydr. Res.*, 2007, **342**(14), 2067–2074, DOI: 10.1016/j.carres.2007.05.022.
45 J. Q. Albarelli, D. T. Santos, S. Murphy and M. Oelgemöller, Use of Ca–Alginate as a Novel Support for TiO2 Immobilization in Methylene Blue Decolorisation, *Water Sci. Technol.*, 2009, **60**(4), 1081–1087, DOI: 10.2166/wst.2009.459.
46 M. Abbas, Z. Harrache and M. Trari, Mass-Transfer Processes in the Adsorption of Crystal Violet by Activated Carbon Derived from Pomegranate Peels: Kinetics and Thermodynamic Studies, *J. Eng. Fibers Fabrics*, 2020, **15**, 1558925020919847, DOI: 10.1177/1558925020919847.

47 Y. Song, R. Peng, S. Chen and Y. Xiong, Adsorption of Crystal Violet onto Epichlorohydrin Modified Corncob, *Desalination Water Treat.*, 2019, **154**, 376–384, DOI: 10.5004/dwt.2019.24067.

48 H. Behloul, H. Ferkous, N. Bougdah, S. Djellali, M. Alam, C. Djilani, A. Sedik, D. Lerari, B.-H. Jeon and Y. Benguerba, New Insights on the Adsorption of CI-Reactive Red 141 Dye Using Activated Carbon Prepared from the ZnCl2-Treated Waste Cotton Fibers: Statistical Physics, DFT, COSMO-RS, and AIM Studies, *J. Mol. Liq.*, 2022, **364**, 119956, DOI: 10.1016/j.molliq.2022.119956.

49 M. Khelfaoui, D. Zouied, N. Bouzenad, A. Abdennouri, I. Boussouf, M. Damous, R. N. Boucetta, F. A. Merzeg, A. Djermoune and Y. Belhocine, Antimicrobial Activity and High Anticorrosion Efficiency of Carpobrotus Acinaciformis L. Extracts Against C1020 Carbon Steel Corrosion in a Hydrochloric Acid Medium, *Chem. Biochem. Eng. Q.*, 2025, **39**(1), 1–13, DOI: 10.15255/CABEQ.2024.2397.

50 M. Hussain, M. A. Ansari and F. A. Mir, Preparation, Characterization and Cooling Performance of ZnO Based Nanofluids, *Discov. Appl. Sci.*, 2024, **6**(3), 92, DOI: 10.1007/s42452-024-05705-8.

51 A. R. Pradipta and A. Irunsah, Synthesis of Modified TiO_2 Nanocomposite Using Fe_3O_4 and Nickel as Photocatalyst in Reduction of Silver Ions, *Indones. J. Chem. Stud.*, 2022, **1**(1), 8–12, DOI: 10.55749/ijcs.v1i1.7.

52 M. M. Khalaf, E. Da'na, K. Al-Amer and M. Hessien, Experimental Design Modeling of the Effect of Hexagonal Wurtzite—ZnO Synthesis Conditions on Its Characteristics and Performance as a Cationic and Anionic Adsorbent, *Molecules*, 2019, **24**(21), 3884, DOI: 10.3390/molecules24213884.

53 Y. Nosaka and A. Y. Nosaka, Generation and Detection of Reactive Oxygen Species in Photocatalysis, *Chem. Rev.*, 2017, **117**(17), 11302–11336, DOI: 10.1021/acs.chemrev.7b00161.

54 P. Porrawatkul, R. Pimsen, A. Kuyyogsuy, P. Rattanaburi and P. Nuengmatcha, Morphology-Dependent Photocatalytic Performance of ZnO Nanostructures in Organic Dye and Antibiotic Degradation, *Int. J. Sci. Environ. Technol.*, 2024, **21**(11), 7397–7414, DOI: 10.1007/s13762-024-05530-x.

55 D. P. Singh, B. Sirota, S. Talpatra, P. Kohli, C. Rebholz and S. M. Aouadi, Broom-like and Flower-like Heterostructures of Silver Molybdate through pH Controlled Self Assembly, *J. Nanopart. Res.*, 2012, **14**(4), 781, DOI: 10.1007/s11051-012-0781-0.

56 C. B. Ong, L. Y. Ng and A. W. Mohammad, A Review of ZnO Nanoparticles as Solar Photocatalysts: Synthesis, Mechanisms and Applications, *Renew. Sustain. Energy Rev.*, 2018, **81**, 536–551, DOI: 10.1016/j.rser.2017.08.020.

57 H. Gao, D. Zhang, M. Yang and S. Dong, Photocatalytic Behavior of Fluorinated Rutile TiO2(110) Surface: Understanding from the Band Model, *Sol. RRL*, 2017, **1**(12), 1700183, DOI: 10.1002/solr.201700183.

58 M. A. Borysiewicz, ZnO as a Functional Material, a Review, *Crystals*, 2019, **9**(10), 505, DOI: 10.3390/cryst9100505.

59 S. Huo, S. Ding, C. Zhao, C. Wang, F. Yu, J. Fang and Y. Yang, Growth and Photocatalytic Activities of Porous ZnO/TiO2 Composite Microspheres with Crystalline–Amorphous Phase Boundary, *Catal. Lett.*, 2021, **151**(7), 1937–1947, DOI: 10.1007/s10562-020-03463-x.

60 M. A. Habib, M. T. Shahadat, N. M. Bahadur, I. M. I. Ismail and A. J. Mahmood, Synthesis and Characterization of ZnO-TiO2 Nanocomposites and Their Application as Photocatalysts, *Int. Nano Lett.*, 2013, **3**(1), 5, DOI: 10.1186/2228-5326-3-5.

61 M. Zaker Mobaraki and A. Haghighatzadeh, TiO2–ZnO Nanocomposites: Synthesis, Linear and Nonlinear Optical Analysis, *Bull. Mater. Sci.*, 2020, **43**(1), 297, DOI: 10.1007/s12034-020-02256-7.

62 Z. Bourechech, A. Seghier and A. Mokhtar, Assessment of Physically Treated Banana Leaves as a Low-Cost and Eco-Friendly Adsorbent for Removal of a Textile Azo Dye, *Biomass Convers. Biorefin.*, 2023, **13**(15), 14241–14252, DOI: 10.1007/s13399-023-03997-1.

63 I. Loulidi, F. Boukhlifi, M. Ouchabi, A. Amar, M. Jabri, A. Kali, S. Chraibi, C. Hadey and F. Aziz, Adsorption of Crystal Violet onto an Agricultural Waste Residue: Kinetics, Isotherm, Thermodynamics, and Mechanism of Adsorption, *Sci. World J.*, 2020, **2020**(1), 5873521, DOI: 10.1155/2020/5873521.

64 M. Bendjama, O. Hamdaoui, H. Ferkous and A. Alghyamah, Removal of Safranin O from Water by UV/TiO2/IO3− Advanced Oxidation Process: Parametric Study and Impact of Inorganic Ions and Humic Acid, *Catalysts*, 2023, **13**(2), 447, DOI: 10.3390/catal13020447.

65 K. K. Kaya, C. Orak and S. Horoz, Enhanced Photovoltaic Performance of TiO2 Photoanodes via Surface Modification with ZnFe-Layered Double Hydroxides, *J. Photochem. Photobiol. Chem.*, 2026, **473**, 116863, DOI: 10.1016/j.jphotochem.2025.116863.

66 S. Sultana, K. Islam, Md. A. Hasan, H. M. J. Khan, M. A. R. Khan, A. Deb, Md. Al Raihan and Md. W. Rahman, Adsorption of Crystal Violet Dye by Coconut Husk Powder: Isotherm, Kinetics and Thermodynamics Perspectives, *Environ. Nanotechnol. Monit. Manag.*, 2022, **17**, 100651, DOI: 10.1016/j.enmm.2022.100651.

67 D. Kanakaraju, N. R. Shahdad, M. bt, Y.-C. Lim and A. Pace, Magnetic Hybrid TiO2/Alg/FeNPs Triads for the Efficient Removal of Methylene Blue from Water, *Sustain. Chem. Pharm.*, 2018, **8**, 50–62, DOI: 10.1016/j.scp.2018.02.001.

68 N. Hamrouche, C. Djilani, P. Magri, Y. Belhocine, F. Djazi, M. Kezzar and N. Bouzenad, A Novel Biosorbent from Raw Pomegranate Peel Modified with SnCl2/FeCl2 for the Adsorption of Crystal Violet Cationic Dye: Response Surface Methodology Process Optimization, Thermodynamic, Kinetic, Isotherm, and Recyclability Studies, *Biomass Convers. Biorefin.*, 2024, DOI: 10.1007/s13399-024-05737-5.

69 F. Bouaziz, M. Koubaa, F. Kallel, R. E. Ghorbel and S. E. Chaabouni, Adsorptive Removal of Malachite Green from Aqueous Solutions by Almond Gum: Kinetic Study

and Equilibrium Isotherms, *Int. J. Biol. Macromol.*, 2017, **105**, 56–65, DOI: 10.1016/j.ijbiomac.2017.06.106.

70 A. Kali, Y. Dehmani, I. Loulidi, A. Amar, M. Jabri, A. El-kord and F. Boukhlifi, Study of the Adsorption Properties of an Almond Shell in the Elimination of Methylene Blue in an Aquatic, *Moroccan Journal of ChemistryJ. Chem.*, 2022, **10**(3), 509–522, DOI: 10.48317/IMIST.PRSM/morjchem-v10i3.33140.

71 A. H. Jawad and A. S. Abdulhameed, Mesoporous Iraqi Red Kaolin Clay as an Efficient Adsorbent for Methylene Blue Dye: Adsorption Kinetic, Isotherm and Mechanism Study, *Surf. Interfaces*, 2020, **18**, 100422, DOI: 10.1016/j.surfin.2019.100422.

72 W. S. A. El-Yazeed and A. I. Ahmed, Photocatalytic Activity of Mesoporous WO3/TiO2 Nanocomposites for the Photodegradation of Methylene Blue, *Inorg. Chem. Commun.*, 2019, **105**, 102–111, DOI: 10.1016/j.inoche.2019.04.034.

73 C. Djilani, R. Zaghdoudi, F. Djazi, A. Lallam, B. Bouchekima and P. Magri, Comparative Study of Photocatalytic Activity of Nanocomposites Prepared from Biological Wastes and ZnO Nanoparticles, *Desalination Water Treat.*, 2021, **220**, 329–341, DOI: 10.5004/dwt.2021.27000.

74 H. M. F. Freundlich, Over the Adsorption in Solution, *J. Phys. Chem.*, 1906, **57**(385471), 1100–1107.

75 I. Langmuir, The constitution and fundamental properties of solids and liquids. Part I. solids, *J. Am. Chem. Soc.*, DOI: 10.1021/ja02268a002.

76 L. Nouri, S. Hemidouche, A. Boudjemaa, F. Kaouah, Z. Sadaoui and K. Bachari, Elaboration and Characterization of Photobiocomposite Beads, Based on Titanium (IV) Oxide and Sodium Alginate Biopolymer, for Basic Blue 41 Adsorption/Photocatalytic Degradation, *Int. J. Biol. Macromol.*, 2020, **151**, 66–84, DOI: 10.1016/j.ijbiomac.2020.02.159.

77 N. M. Mahmoodi, B. Hayati, M. Arami and H. Bahrami, Preparation, Characterization and Dye Adsorption Properties of Biocompatible Composite (Alginate/Titania Nanoparticle), *Desalination*, 2011, **275**(1), 93–101, DOI: 10.1016/j.desal.2011.02.034.

78 E. C. Lima, A. Hosseini-Bandegharaei, J. C. Moreno-Piraján and I. Anastopoulos, A Critical Review of the Estimation of the Thermodynamic Parameters on Adsorption Equilibria. Wrong Use of Equilibrium Constant in the Van't Hoof Equation for Calculation of Thermodynamic Parameters of Adsorption, *J. Mol. Liq.*, 2019, **273**, 425–434, DOI: 10.1016/j.molliq.2018.10.048.

79 G. Crini and P.-M. Badot, Application of Chitosan, a Natural Aminopolysaccharide, for Dye Removal from Aqueous Solutions by Adsorption Processes Using Batch Studies: A Review of Recent Literature, *Prog. Polym. Sci.*, 2008, **33**(4), 399–447, DOI: 10.1016/j.progpolymsci.2007.11.001.

80 R. Fabryanty, C. Valencia, F. E. Soetaredjo, J. N. Putro, S. P. Santoso, A. Kurniawan, Y.-H. Ju and S. Ismadji, Removal of Crystal Violet Dye by Adsorption Using Bentonite – Alginate Composite, *J. Environ. Chem. Eng.*, 2017, **5**(6), 5677–5687, DOI: 10.1016/j.jece.2017.10.057.

81 A. A. Oladipo and M. Gazi, Enhanced Removal of Crystal Violet by Low Cost Alginate/Acid Activated Bentonite Composite Beads: Optimization and Modelling Using Non-Linear Regression Technique, *J. Water Proc. Eng.*, 2014, **2**, 43–52, DOI: 10.1016/j.jwpe.2014.04.007.

82 A. Aichour and H. Zaghouane-Boudiaf, Synthesis and Characterization of Hybrid Activated Bentonite/Alginate Composite to Improve Its Effective Elimination of Dyes Stuff from Wastewater, *Appl. Water Sci.*, 2020, **10**(6), 146, DOI: 10.1007/s13201-020-01232-0.

83 A. Aichour and H. Zaghouane-Boudiaf, Synthesis and Characterization of Hybrid Activated Bentonite/Alginate Composite to Improve Its Effective Elimination of Dyes Stuff from Wastewater, *Appl. Water Sci.*, 2020, **10**(6), 146, DOI: 10.1007/s13201-020-01232-0.

84 A. Mirza and R. Ahmad, An Efficient Sequestration of Toxic Crystal Violet Dye from Aqueous Solution by Alginate/Pectin Nanocomposite: A Novel and Ecofriendly Adsorbent, *Groundw. Sustain. Dev.*, 2020, **11**, 100373, DOI: 10.1016/j.gsd.2020.100373.

85 K. Akin, V. Ugraskan, B. Isik and F. Cakar, Adsorptive Removal of Crystal Violet from Wastewater Using Sodium Alginate-Gelatin-Montmorillonite Ternary Composite Microbeads, *Int. J. Biol. Macromol.*, 2022, **223**, 543–554, DOI: 10.1016/j.ijbiomac.2022.11.002.

86 A. Djelad, A. Mokhtar, A. Khelifa, A. Bengueddach and M. Sassi, Alginate-Whey an Effective and Green Adsorbent for Crystal Violet Removal: Kinetic, Thermodynamic and Mechanism Studies, *Int. J. Biol. Macromol.*, 2019, **139**, 944–954, DOI: 10.1016/j.ijbiomac.2019.08.068.

87 R. Ahmad and K. Ansari, Fabrication of Alginate@silver Nanoparticles (Alg@AgNPs) Bionanocomposite for the Sequestration of Crystal Violet Dye from Aqueous Solution, *Int. J. Biol. Macromol.*, 2022, **218**, 157–167, DOI: 10.1016/j.ijbiomac.2022.07.092.

88 J. Mittal, R. Ahmad, M. O. Ejaz, A. Mariyam and A. Mittal, A Novel, Eco-Friendly Bio-Nanocomposite (Alg-Cst/Kal) for the Adsorptive Removal of Crystal Violet Dye from Its Aqueous Solutions, *Int. J. Phytoremediation*, 2022, **24**(8), 796–807, DOI: 10.1080/15226514.2021.1977778.

89 S. Pashaei-Fakhri, S. J. Peighambardoust, R. Foroutan, N. Arsalani and B. Ramavandi, Crystal Violet Dye Sorption over Acrylamide/Graphene Oxide Bonded Sodium Alginate Nanocomposite Hydrogel, *Chemosphere*, 2021, **270**, 129419, DOI: 10.1016/j.chemosphere.2020.129419.

90 S. K. Mohamed, Sh. H. Hegazy, N. A. Abdelwahab and A. M. Ramadan, Coupled Adsorption-Photocatalytic Degradation of Crystal Violet under Sunlight Using Chemically Synthesized Grafted Sodium Alginate/ZnO/Graphene Oxide Composite, *Int. J. Biol. Macromol.*, 2018, **108**, 1185–1198, DOI: 10.1016/j.ijbiomac.2017.11.028.

91 R. Arshad, T. Javed and A. Thumma, Exploring the Efficiency of Sodium Alginate Beads and Cedrus Deodara Sawdust for

Adsorptive Removal of Crystal Violet Dye, *J. Dispersion Sci. Technol.*, 2024, **45**(12), 2330–2343, DOI: 10.1080/01932691.2023.2265464.

92 T. Nike, D. Kaushal, V. Chauhan, P. Shandilya and M. Kumar, Development of Guar Gum-Sodium Alginate Based Hydrogel for Sustainable and Efficient Removal of Crystal Violet Dye from Wastewater, *Int. J. Biol. Macromol.*, 2025, **330**(3), 148122, DOI: 10.1016/j.ijbiomac.2025.148122.